DALTON
FULL PAPER

Structure and magnetic properties of tri- and hexa-nuclear hydroxo-bridged copper(II) complexes formed by a trimacrocyclic derivative of 1,4,7-triazacyclononane †

Bim Graham,[a] Leone Spiccia,*[a] Gary D. Fallon,[a] Milton T. W. Hearn,[b] Frank E. Mabbs,[c] Boujemaa Moubaraki[a] and Keith S. Murray[a]

[a] *School of Chemistry, PO Box 23, Monash University, Victoria 3800, Australia*
[b] *Centre for Bioprocess Technology, Department of Biochemistry, P.O. Box 130, Monash University, Victoria 3800, Australia*
[c] *Department of Chemistry, University of Manchester, Manchester, UK M13 9PL*

Received 26th June 2001, Accepted 14th November 2001
First published as an Advance Article on the web 11th February 2002

Two hydroxo-bridged Cu(II) complexes of the trimacrocyclic ligand, 1,3,5-tris(1,4,7-triazacyclonon-1-ylmethyl)-benzene (L^{mes}), have been prepared and characterized. The trinuclear complex, $[Cu_3L^{mes}(\mu\text{-}OH)_2(H_2O)_2](ClO_4)_4\cdot 3.2H_2O$ (**1**), formed when the pH of an aqueous solution of $[Cu_3L^{mes}(H_2O)_6](ClO_4)_6\cdot 6H_2O$, was adjusted to *ca.* 6. X-Ray structural analysis confirmed the presence of a binuclear $[Cu_2(\mu\text{-}OH)_2]^{2+}$ core and an isolated Cu(II) centre. The "roof-shaped" $[Cu_2(\mu\text{-}OH)_2]^{2+}$ core has a dihedral angle (δ) of 152° between the CuO_2 planes and exhibits a relatively short Cu ··· Cu distance of 2.9041(8) Å. An increase in pH to 9.5 generates the hexanuclear complex, $[Cu_6(L^{mes})_2(\mu\text{-}OH_6](ClO_4)_6\cdot 2H_2O$ (**2**), by linking two $[Cu_3L^{mes}(\mu\text{-}OH)_2]^{4+}$ trinuclear units *via* two μ-hydroxo bridges. The structure of **2** features three $[Cu_2(\mu\text{-}OH)_2]^{2+}$ units, two with bent geometries, similar to that observed in **1** [δ = 153°, Cu ··· Cu = 2.8757(8) Å], and one with planar geometry [Cu ··· Cu = 2.961(1) Å]. A variable temperature magnetic susceptibility study on **1** has identified an $S = 1/2$ ground state, consistent with a system composed of an antiferromagnetically coupled Cu(II) pair ($J = -24$ cm^{-1}) and a magnetically isolated Cu(II) centre. Variable temperature Q-band EPR spectra confirmed this interpretation. Comparisons to the Q-band EPR spectra of the previously reported trinuclear complex, $\{[Cu_3L^{mes}(\mu\text{-}OH)(\mu_3\text{-}HPO_4)(H_2O)](PF_6)_3\cdot 3H_2O\}_n$, were made, the latter also shows a $S = 1/2$ ground state but with the unpaired electron delocalised between two Cu(II) ions. The susceptibility data for **2** were interpreted in terms of the presence of three independent Cu(II) binuclear units with weak antiferromagnetic coupling observed in both the bent and planar $[Cu_2(\mu\text{-}OH)_2]^{2+}$ cores ($J = -61$ and -29 cm^{-1}, respectively).

Introduction

Polynuclear Cu(II) complexes form an extremely active area of research in modern coordination chemistry. The impetus for these studies derives from many quarters, with one major focus being on the development of correlations between molecular structure and magnetic behavior. Hydroxo-bridged binuclear Cu(II) complexes have featured prominently in these studies,[1–10] with Hodgson and Hatfield noting a correlation between the exchange coupling constant, J, and the Cu–O–Cu angle in complexes with planar or near-planar $[Cu_2(\mu\text{-}OH)_2]^{2+}$ cores.[4,7] Evidence that other structural parameters may also influence the magnitude and sign of J continues to stimulate interest in binuclear complexes, especially those which feature unusual $[Cu_2(\mu\text{-}OH)_2]^{2+}$ core geometries.[5–7,10]

Polynuclear copper complexes have also been actively pursued as models for multi-copper units found at the active sites of important biological proteins.[11–18] Through the preparation of low molecular weight complexes, which mimic the structure, properties and/or function of these bio-sites, valuable insights into the electronic and structural features responsible for the spectral and magnetic properties of Cu enzymes can be achieved, as well as an understanding of mechanistic aspects of their mode of operation. Although binuclear copper complexes have featured most prominently in these studies, the presence of triangular arrays of copper centres at the active sites of enzymes such as ascorbate oxidase, laccase and ceruplasmin[14] has led to increased interest in trinuclear complexes.[17–26]

We have recently reported on the ability of the trinucleating ligand, L^{mes}, consisting of three 1,4,7-triazacyclononane (tacn) macrocycles linked by a mesitylene unit, to act as a template to models for the trinuclear sites of multi-copper oxidases. The ligand facilitated the self-assembly of a novel polymeric Cu(II) complex containing asymmetric trinuclear sites in which three Cu(II) centres are linked by a phosphate bridge.[25] Our general interest in polynuclear metal complexes[25,27–33] has led us to use L^{mes} in the synthesis of two hydroxo-bridged Cu(II) complexes, $[Cu_3L^{mes}(\mu\text{-}OH)_2(H_2O)_2](ClO_4)_4\cdot 3.2H_2O$ (**1**) and $[Cu_6(L^{mes})_2(\mu\text{-}OH)_6](ClO_4)_6\cdot 2H_2O$ (**2**). The X-ray structures, which have revealed the presence "roof-shaped" $[Cu_2(\mu\text{-}OH)_2]^{2+}$ cores, and magnetic properties of **1** and **2** are reported.

Experimental

Materials and reagents

Reagent or analytical grade materials were obtained from commercial suppliers and used as received. The nonahydrobromide salt of 1,3,5-tris(1,4,7-triazacyclonon-1-ylmethyl)benzene ($L^{mes}\cdot 9HBr$), $[Cu_3L^{mes}(H_2O)_6](ClO_4)_6\cdot 3H_2O$ and $\{[Cu_3L^{mes}(\mu\text{-}OH)(\mu_3\text{-}HPO_4)(H_2O)](PF_6)_3\cdot 3H_2O\}_n$ were available from our previous work.[25]

Physical measurements

Infrared spectra were recorded on a Perkin Elmer 1600 FTIR spectrophotometer as KBr pellets or Nujol mulls, and electronic

† Electronic supplementary information (ESI) available: Q-band EPR spectra (34.1 GHz) measured on a powder sample of $\{[Cu_3L(\mu\text{-}OH)(\mu_3\text{-}HPO_4)(H_2O)](PF_6)_3\cdot 3H_2O\}_n$ at: (a) 200 K; (b) 114 K; (c) 4 K. See http://www.rsc.org/suppdata/dt/b1/b105595j/

 DOI: 10.1039/b105595j

spectra on a Cary 5 spectrophotometer. Electron microprobe analyses were made with a JEOL JSM-1 scanning electron microscope through an NEC X-ray detector and pulse-processing system connected to a Packard multichannel analyser. Variable temperature magnetic susceptibility measurements were made using a Quantum Design MPMS SQUID magnetometer operating in an applied field of 1 Tesla. Samples of **1** and **2** from the batches that were subjected to characterization studies, and from which a crystal of each complex was selected for X-ray crystallography, were powdered and used in magnetic studies. The powdered samples were contained in calibrated gelatine capsules which were held in the centre of a straw, the latter being attached to the end of the sample rod. The temperature and field were checked against a standard Pd sample and $CuSO_4 \cdot 5H_2O$. Fitting of the magnetic data employed a non-linear least squares program called POLYMER written at Monash University. Variable temperature Q-band ESR spectra were recorded at Manchester University on a Bruker ESP-300E-12/15 Z instrument operating at the microwave frequencies of 33.94 GHz (**1**) and 34.1 GHz ($\{[Cu_3L\text{-}(\mu\text{-}OH)(\mu_3\text{-}HPO_4)(H_2O)](PF_6)_3 \cdot 3H_2O\}_n$). Typical instrument settings were: receiver gain, 500; modulation frequency, 100 KHz; modulation amplitude, 10 G; microwave power, variable.

CAUTION! Although no problems were encountered in this work, transition metal perchlorates are potentially explosive and should be prepared in small quantities and handled with care.

Preparations

$[Cu_3L^{mes}(\mu\text{-}OH)_2(H_2O)_2](ClO_4)_4 \cdot 3.2H_2O$ (1). To a solution of $Cu(NO_3)_2 \cdot 3H_2O$ (0.61 g, 2.5 mmol) and $L^{mes} \cdot 9HBr$ (1.00 g, 0.813 mmol) was added NaOH (2 M) until copper hydroxide began to precipitate. Sufficient dilute HCl (2 M) was then added to just dissolve this precipitate. The resulting dark blue solution was diluted to 2 L with water and loaded onto a Sephadex SP-C25 column (H^+ form, 15 cm × 4 cm). After washing the column with H_2O and 0.2 M $NaClO_4$ solution to remove a light green band of excess Cu^{2+}, a dark blue band was eluted with 1.0 M $NaClO_4$ solution. Evaporation of this solution yields $[Cu_3L^{mes}(H_2O)_6](ClO_4)_6 \cdot 6H_2O$ (**3**).[25] Crystals of (**1**) suitable for X-ray crystallography were deposited from a solution of $[Cu_3L^{mes}(H_2O)_6]^{6+}$, which had been purified by CEC (cation exchange chromatography), a few days following adjustment of the pH to 6 (from *ca.* 4) with 2M NaOH. These were collected by filtration, washed with MeOH and air-dried. The crystals became "frosty" during drying, indicating some loss of solvent of crystallization. Yield 0.21 g (43%). Anal. Calc. for $C_{27}H_{63.4}Cl_4Cu_3N_9O_{23.2}$ $\{[Cu_3L^{mes}(OH)_2(H_2O)_2](ClO_4)_4 \cdot 3.2H_2O\}$: C, 26.6; H, 5.2; N, 10.4. Found: C, 27.0; H, 5.3; N, 10.5%. Electron microprobe: Cu, Cl present. UV-Visible spectrum (H_2O, pH ≈ 6.5): λ_{max}/nm (ε_{max} per Cu/M^{-1} cm^{-1}), 623 (72), ≈880 sh. Selected IR bands (KBr, cm^{-1}): 3442s br, 3310m, 2927w, 1638m br, 1493w, 1459m, 1147vs, 1118vs, 1086vs, 943w, 628s.

$[Cu_6(L^{mes})_2(\mu\text{-}OH)_6](ClO_4)_6 \cdot 2H_2O$ (2). *Method A.* A solution of $[Cu_3L^{mes}(H_2O)_6](ClO_4)_6 \cdot 6H_2O$ (0.20 g, 0.13 mmol) in H_2O (10 mL) was heated on a steam bath and the pH adjusted to 9.5 with NaOH solution (2 M). $NaClO_4$ (1.00 g, 8.17 mmol) was then added and the solution left to stand. The fine blue precipitate of **2** that formed was collected by filtration, washed with MeOH and air-dried. Yield 0.10 g, 69%.

Method B. To a solution of $[Cu_3L^{mes}(H_2O)_6](ClO_4)_6 \cdot 6H_2O$ (0.0317 g, 0.0211 mmol) in H_2O (2 mL) was added Na_2CO_3 (0.0024 g, 0.023 mmol). Dark blue crystals suitable for X-ray crystallography were deposited over a few days. Yield 0.010 g, 44%. Anal. Calc. for $C_{54}H_{120}Cl_6Cu_6N_{18}O_{36}$ $\{[Cu_6(L^{mes})_2(OH)_6](ClO_4)_6 \cdot 2H_2O\}$: C, 30.6; H, 5.7; N, 11.9. Found: C, 29.6; H, 5.5; N, 11.6%. Electron microprobe: Cu, Cl present. UV-Visible spectrum (H_2O): λ_{max}/nm (ε_{max} per Cu/M^{-1} cm^{-1}), [pH = 9.1 (CHES buffer) 345 (222), 614 (79), ≈880sh]; [pH = 7.6 (MOPS buffer) 345 (185), 617 (77), ≈880sh]; [pH = 4.4 (KH phthalate buffer), 628 (93), 990(32)]. Selected IR bands (KBr, cm^{-1}): 3424s br, 3306s, 2935m, 1638m, 1460m, 1400w, 1091vs br, 626s.

Table 1 Crystallographic data for **1** and **2**

Chemical formula	$C_{27}H_{63.4}Cl_4Cu_3N_9O_{23.2}$	$C_{54}H_{112}Cl_6Cu_6N_{18}O_{32}$
M/g mol^{-1}	1217.89	2119.57
Crystal system	Triclinic	Monoclinic
Space group	$P\bar{1}$ (no. 2)	$P2_1/a$
a/Å	12.1020(5)	14.4299(4)
b/Å	13.6888(7)	13.9410(6)
c/Å	17.053(1)	21.463(1)
α/°	67.028(1)	90
β/°	72.983(1)	109.377(1)
γ/°	67.912(1)	90
V/Å^3	2374.6(2)	4073.1(3)
Z	2	2
T/K	173	173
λ/Å	0.71069	0.71069
D_c/g cm^{-3}	1.703	1.728
μ(MoKα)/cm^{-1}	16.45	18.28
No. data measured	21040	34456
No. data ($I \geq 3\sigma(I)$)	6897	6913
R	0.049[a]	0.056[a]
R'	0.057[b]	0.070[b]
ρ_{min}, ρ_{max}/e Å^{-3}	−0.88, 1.48	−1.29, 1.46

[a] $R = \Sigma(||F_o| - |F_c||)/\Sigma|F_o|$. [b] $R' = [\Sigma w(|F_o| - |F_c|)^2/\Sigma wF_o^2]^{1/2}$, where $w = [\sigma^2(F_o)]^{-1}$.

X-Ray crystallography

Intensity data for blue crystals of **1** (dimensions ≈ 0.20 × 0.10 × 0.10 mm) and **2** (dimensions ≈ 0.14 × 0.12 × 0.10 mm) were measured at 173 K on a Nonius Kappa CCD fitted with graphite-monochromated Mo-Kα radiation (0.71069 Å). Data were collected to a maximum 2θ value of 60.2 and 59.5°, respectively and processed using the Nonius software. The structures were solved by direct methods and expanded using standard Fourier routines in the teXsan software package.[34] All non-hydrogen atoms were refined with anisotropic thermal parameters. Hydrogens, except those of water molecules, were included in calculated positions but not refined. Neutral atom scattering factors were those incorporated in the teXsan program. Refinement was against F [sigma weights, *i.e.*, $1/\sigma^2(F)$]. For **1**, the thermal parameters for the oxygens on the waters of crystallization were set to reasonable numbers and the occupancy refined over five positions (O(24) 0.7; O(25) 1; O(26) 0.8; O(27) 0.5; O(28) 0.2). Crystal parameters and details of the data collection, solution and refinement are summarised in Table 1. ORTEP perspectives of the complexes are presented in Fig. 1 and 2, and selected bond lengths and angles in Tables 2 and 3.

CCDC reference numbers 174283 and 174284.

See http://www.rsc.org/suppdata/dt/b1/b105595j/ for crystallographic data in CIF or other electronic format.

Results and discussion

Synthesis and characterization

Mixing of $L^{mes} \cdot 9HBr$ with *ca.* three molar equivalents of $Cu(NO_3)_2 \cdot 3H_2O$, followed by pH adjustment and purification by cation exchange chromatography yields blue crystals of $[Cu_3L^{mes}(H_2O)_6](ClO_4)_6 \cdot 6H_2O$ (**3**), after evaporation.[25] As outlined in Scheme 1, adjustment of the pH of the eluate to 6, prior to crystallization of **3**, leads to hydroxo-bridge formation between two of the Cu(II) centres, with the third remaining coordinated to two terminal water ligands. Slow evaporation crystallized this "partially-bridged" complex as the perchlorate salt, $[Cu_3L^{mes}(\mu\text{-}OH)_2(H_2O)_2](ClO_4)_4 \cdot 3.2H_2O$ (**1**) (waters of

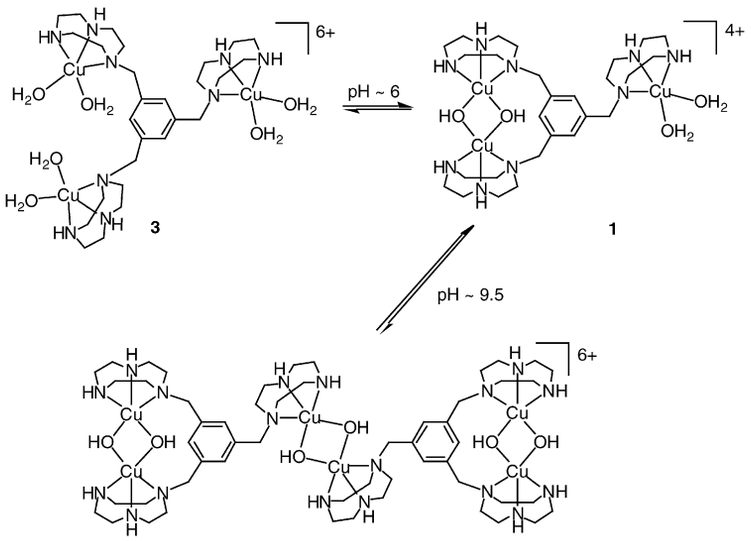

Scheme 1

hydration from crystallographic refinement). A further increase in pH to 9.5 promotes hydroxo-bridge formation between two trinuclear units of **1** (see Scheme 1) and the rapid precipitation of a "fully-bridged" hexanuclear complex, $[Cu_6(L^{mes})_2(\mu\text{-}OH)_6](ClO_4)_6\cdot 2H_2O$ (**2**).

Analytical and electron microprobe data for **1** and **2** were consistent with the proposed compositions and the IR spectra exhibited the bands expected for these complexes. Bands due specifically to OH stretching of the hydroxo bridges were masked by strong ν(OH) stretches attributable to water ligands and/or water of crystallization water. The UV-Visible spectrum of **2** recorded in water at pH = 9.1 shows a broad d–d band centred at 614 nm with a high energy shoulder at *ca.* 880 nm, in agreement with a $(d_{x^2-y^2})^1$ electronic ground-state of a Cu(II) ion in a square pyramidal (SP) geometry, for which $d_{z^2} \longrightarrow d_{x^2-y^2}$ and d_{xz}, $d_{yz} \longrightarrow d_{x^2-y^2}$ transitions are expected.[35] Apart from changes in position of these bands reflecting variations in ligand field strength, the spectra of **2** and **3** are also consistent with the presence of Cu(II) in SP geometry. The variable pH spectra, recorded for **2** at pH = 4.4, 7.6 and 9.1 (see Experimental section) revealed that **1**, **2** and **3** can be interconverted by pH adjustment (Scheme 1). **3** dominates at low pH and **2** at high pH. At neutral pHs, the spectra indicate that a mixture of two and possibly all three complexes may be co-existing.

Crystal structures

The "dimer-plus-monomer" structure proposed for **1** was confirmed through a single crystal X-ray structure determination, which showed that the crystals are composed of discrete $[Cu_3L^{mes}(\mu\text{-}OH)_2(H_2O)_2]^{4+}$ cations (see Fig. 1), perchlorate anions and waters of crystallization.

Each cationic unit incorporates three Cu(II) centres coordinated by the L^{mes} ligand. Two of the three Cu(II) centres are linked by a pair of hydroxo bridges. The third Cu(II) centre is terminally coordinated by two water molecules and resides on the opposite side of the plane of the central aromatic ring, so that the complex adopts a "chair-like" conformation with large Cu(3) ··· Cu(1) and Cu(3) ··· Cu(2) separations (>9 Å). All three copper(II) centres exhibit pseudo-SP geometries with τ values[36] of ≤16%. In each case, two secondary amines and two oxygen donors occupy the four basal coordination sites and a tertiary bridgehead nitrogen resides in the apical position. The Cu(1), Cu(2) and Cu(3) centres are displaced from the corresponding basal planes by 0.16, 0.16 and 0.10 Å, respectively. The basal Cu–N bonds are all shorter than the associated axial Cu–N bonds by 0.26 to 0.38 Å.

In contrast to the planar $[Cu_2(\mu\text{-}OH)_2]^{2+}$ core observed in $[Cu_2(Me_3tacn)_2(\mu\text{-}OH)_2](ClO_4)_2$[37] and many similar "unsupported" hydroxo-bridged dimers,[1–4,7,10] the $[Cu_2(\mu\text{-}OH)_2]^{2+}$ unit in **1** is bent or "roof-shaped". This distortion is evident from the dihedral angle between the Cu(1)/O(1)/O(2) and Cu(2)/O(1)/O(2) planes (152°) and results in a shorter Cu ··· Cu separation [2.9041(8) Å] than is typically found in unsupported dimers {*e.g.*, 2.971(1) Å in $[Cu_2(Me_3tacn)_2(\mu\text{-}OH)_2](ClO_4)_2$}.[37] Bent $[Cu_2(\mu\text{-}OH)_2]^{2+}$ cores have been found in $[Cu_4L^{dur}(\mu\text{-}OH)_4](ClO_4)_4$ [L^{dur} = 1,2,4,5-tetrakis(1,4,7-triazacyclonon-1-ylmethyl)benzene],[33] $[Cu_2(C_6H_{11}NH_2)_4(\mu\text{-}OH)_2](ClO_4)_2$[5] and $[Cu_2(CH_3NH_2)_4(\mu\text{-}OH)_2](SO_4)\cdot H_2O$,[6] which show dihedral angles of 159, 148 and 133° and Cu ··· Cu distances of 2.939(9), 2.934(8) and 2.782(5) Å, respectively. In the latter two complexes, monodentate amine ligands cap the $[Cu_2(\mu\text{-}OH)_2]^{2+}$ core. Notably, the perturbation of the $[Cu_2(\mu\text{-}OH)_2]^{2+}$ core in **1** may not arise from constraints imposed by the mesitylene tether since the $[Cu_2(\mu\text{-}OH)_2]^{2+}$ core in $[Cu_2L^{mx}(\mu\text{-}OH)_2](BPh_4)_2$ [L^{mx} = 1,3-bis(1,4,7-triazacyclonon-1-ylmethyl)benzene], is supported by a similar backbone but is only very slightly bent with a dihedral angle of 174° and a Cu ··· Cu separation of 2.9464(5) Å.[38]

The longer Cu–O(2) distances [2.019(3) and 2.015(3) Å] *cf.* Cu–O(1) distances [1.900(4) and 1.922(3) Å] may be reflecting distortion of the $[Cu_2(\mu\text{-}OH)_2]^{2+}$ core in **1**, although it should be noted that O(2) does exhibit a high degree of thermal motion. The Cu(1)–O(2)–Cu(2) angle [92.1(1)°] appears more acute than the Cu(1)–O(1)–Cu(2) angle [98.9(2)°]. Similar distortions are observed in $[Cu_4L^{dur}(\mu\text{-}OH)_4](ClO_4)_4$,[33] $[Cu_2(C_6H_{11}NH_2)_4(\mu\text{-}OH)_2](ClO_4)_2$[5] and $[Cu_2(CH_3NH_2)_4(\mu\text{-}OH)_2](SO_4)\cdot H_2O$,[6] while the cores in $[Cu_2L^{mx}(\mu\text{-}OH)_2](BPh_4)_2$[38] and $[Cu_2(Me_3tacn)_2(\mu\text{-}OH)_2](ClO_4)_2$[37] are symmetrical with regards to the Cu–O bond lengths and Cu–O–Cu angles. The distortion in bond lengths seems to be associated with the bending of the $[Cu_2(\mu\text{-}OH)_2]^{2+}$ core. Crystal packing effects or H-bonding interactions could also be contributing. In **1**, one OH bridge forms a moderately strong H-bond to a water molecule [O(2) ··· O(4) = 2.64 Å] and interacts weakly with a perchlorate anion [O(2) ··· O(15) = 3.16 Å], whilst the other participates in only one H-bond contact with a perchlorate anion [O(1) ··· O(26) = 2.68 Å].

A further noteworthy feature is that tethering of the tacn rings in L^{mes}, L^{dur} and L^{mx} enforces a *cisoid* arrangement of the two edge-sharing CuN_3O_2 polyhedra in the "dimeric" units of **1**, $[Cu_4L^{dur}(\mu\text{-}OH)_4](ClO_4)_4$[33] and $[Cu_2L^{mx}(\mu\text{-}OH)_2](BPh_4)_2$.[38] The two apical bridgehead nitrogens lie on the same side of the $Cu_2(\mu\text{-}OH)_2^{2+}$ unit. In contrast, the Me_3tacn capped Cu(II)

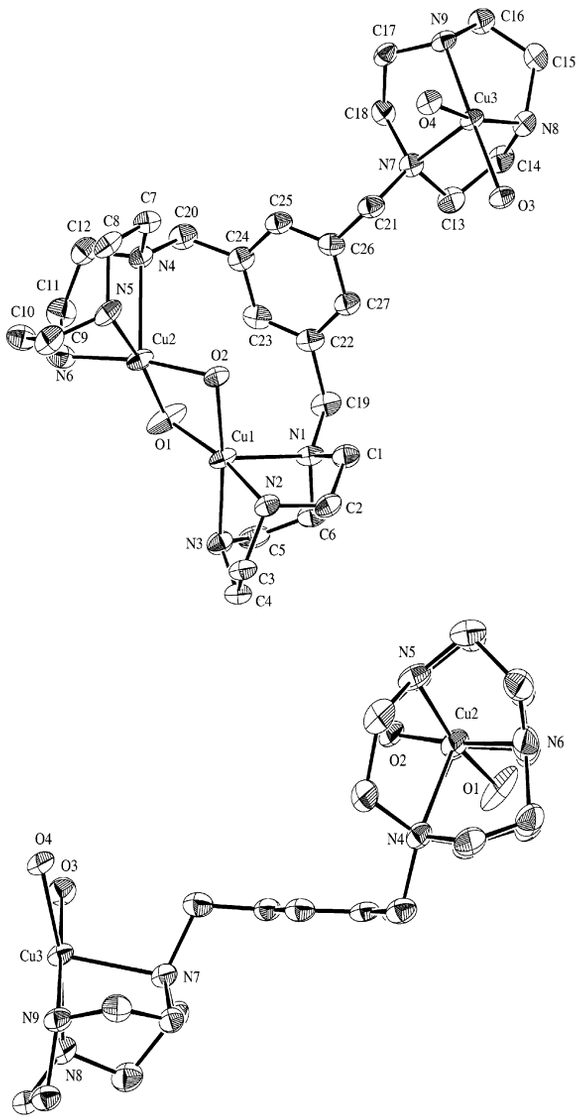

Fig. 1 ORTEP plots of the molecular cation in **1** with the atomic labelling scheme. The "side-on" view shows the "chair-like" conformation of the L^{mes} ligand and the bending of the hydroxo bridges toward the mesitylene spacer.

dimer is centrosymmetric, with the apical nitrogens adopting a *transoid* conformation with respect to the Cu_2O_2 plane.[37]

A single crystal X-ray structure determination of **2** confirmed that di-μ-hydroxo-bridge formation between the Cu(3) centres of two cations found in **1** has resulted in the assembly of the hexanuclear units of $[Cu_6(L^{mes})_2(\mu\text{-}OH)_6]^{4+}$ (see Fig. 2). The complex is centrosymmetric about the midpoint of the central $[Cu_2(\mu\text{-}OH)_2]^{2+}$ unit and each Cu(II) centre resides in slightly distorted SP geometry, with τ values ≤10%. Again two secondary amines and two hydroxo groups form the basal plane around each Cu(II) centre and the tertiary bridgehead nitrogen is in the apical position. The average Cu–N(basal) bonds are ≈ 0.30 Å shorter than the Cu–N(apical) bonds. The Cu(II) centres are displaced from their basal planes by ≈ 0.20 Å.

The geometry of the central "dimer" unit in **2** is reminiscent of that in $[Cu_2(Me_3tacn)_2(\mu\text{-}OH)_2](ClO_4)_2$,[37] with the Cu(II) centres and bridging oxygens being co-planar and the two apical nitrogens adopting a *trans* configuration with respect to the plane of these atoms. Not surprisingly, the Cu ··· Cu distances for these two structures are identical [2.961(2) Å for **2** *vs.* 2.971(1) Å]. Somewhat shorter separations are found for the other two $[Cu_2(\mu\text{-}OH)_2]^{2+}$ units in **2** [Cu ··· Cu = 2.8757(8) Å], which exhibit bent conformations and a dihedral angle [153° between the Cu(1)/O(1)/O(2) and Cu(2)/O(1)/O(2) planes] similar to that observed for **1**.

Table 2 Selected bond distances (Å) and angles (°) for **1**

Cu(1) ··· Cu(2)	2.9041(8)	Cu(1)–O(1)	1.900(4)
Cu(1)–O(2)	2.019(3)	Cu(1)–N(1)	2.358(4)
Cu(1)–N(2)	2.015(4)	Cu(1)–N(3)	2.049(4)
Cu(2)–O(1)	1.922(3)	Cu(2)–O(2)	2.015(3)
Cu(2)–N(4)	2.383(4)	Cu(2)–N(5)	2.007(4)
Cu(2)–N(6)	2.025(5)	Cu(3)–O(3)	2.002(3)
Cu(3)–O(4)	2.020(3)	Cu(3)–N(7)	2.284(4)
Cu(3)–N(8)	2.024(4)	Cu(3)–N(9)	2.005(4)
O(1)–Cu(1)–O(2)	80.7(1)	O(1)–Cu(1)–N(1)	111.5(2)
O(1)–Cu(1)–N(2)	166.7(2)	O(1)–Cu(1)–N(3)	96.1(2)
O(2)–Cu(1)–N(1)	106.0(1)	O(2)–Cu(1)–N(2)	97.7(1)
O(2)–Cu(1)–N(3)	173.4(2)	N(1)–Cu(1)–N(2)	81.7(1)
N(1)–Cu(1)–N(3)	80.5(2)	N(2)–Cu(1)–N(3)	84.1(2)
O(1)–Cu(2)–O(2)	80.3(1)	O(1)–Cu(2)–N(4)	110.0(2)
O(1)–Cu(2)–N(5)	168.6(2)	O(1)–Cu(2)–N(6)	95.3(2)
O(2)–Cu(2)–N(4)	107.6(1)	O(2)–Cu(2)–N(5)	98.4(1)
O(2)–Cu(2)–N(6)	171.7(1)	N(4)–Cu(2)–N(5)	81.2(1)
N(4)–Cu(2)–N(6)	80.6(2)	N(5)–Cu(2)–N(6)	84.5(2)
O(3)–Cu(3)–O(4)	88.5(1)	O(3)–Cu(3)–N(7)	98.5 (1)
O(3)–Cu(3)–N(8)	94.0(1)	O(3)–Cu(3)–N(9)	178.6(2)
O(4)–Cu(3)–N(7)	107.4(1)	O(4)–Cu(3)–N(8)	169.1(1)
O(4)–Cu(3)–N(9)	92.5(1)	N(7)–Cu(3)–N(8)	82.8(2)
N(7)–Cu(3)–N(9)	82.2(1)	N(8)–Cu(3)–N(9)	84.9(2)
Cu(1)–O(1)–Cu(2)	98.9(2)	Cu(1)–O(2)–Cu(2)	92.1(1)

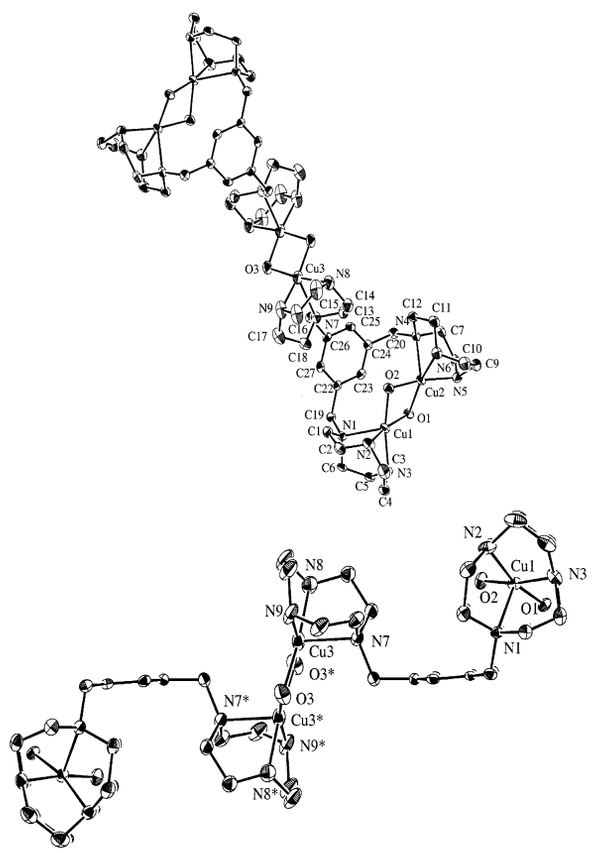

Fig. 2 ORTEP plot of the molecular cation in **2** with the atomic labelling scheme. The lower view shows the planar geometry of the central "dimer", the bent geometry of the flanking "dimers", and the "all-*cis*" conformation of the L^{mes} ligands.

Within each of the "roof-shaped" $[Cu_2(\mu\text{-}OH)_2]^{2+}$ units in **2**, the two Cu–O–Cu angles are slightly different [94.7(1) *vs.* 97.0(1)°] and the Cu–O bonds involving one of the hydroxo groups are slightly longer [1.957(3) and 1.954(4) for O(1) *vs.* 1.920(3) and 1.919(3) Å for O(2)]. These smaller differences, when compared to those observed in **1**, may be reflecting the fact that in **2** the two hydroxo groups are involved in weaker H-bonding interactions with perchlorate anions [O(1) ··· O(5) = 3.21 Å, O(2) ··· O(9) = 2.98 Å] than found in **1**. The symmetry of the complex dictates that the two Cu–O–Cu bond

Table 3 Selected bond distances (Å) and angles (°) for **2**

Cu(1) ··· Cu(2)	2.8757(8)	Cu(3) ··· Cu(3)#1 [a]	2.961(2)
Cu(1)–O(1)	1.957(3)	Cu(1)–O(2)	1.920(3)
Cu(1)–N(1)	2.342(4)	Cu(1)–N(2)	2.037(4)
Cu(1)–N(3)	2.024(4)	Cu(2)–O(1)	1.954(3)
Cu(2)–O(2)	1.919(4)	Cu(2)–N(4)	2.317(4)
Cu(2)–N(5)	2.030(4)	Cu(2)–N(6)	2.029(4)
Cu(3)–O(3)	1.933(4)	Cu(3)–O(3)#1	1.969(4)
Cu(3)–N(7)	2.301(4)	Cu(3)–N(8)	2.020(5)
Cu(3)–N(9)	2.033(5)		
O(1)–Cu(1)–O(2)	80.6(1)	O(1)–Cu(1)–N(1)	113.1 (1)
O(1)–Cu(1)–N(2)	165.2(2)	O(1)–Cu(1)–N(3)	95.9(2)
O(2)–Cu(1)–N(1)	110.3(1)	O(2)–Cu(1)–N(2)	96.8(2)
O(2)–Cu(1)–N(3)	168.7(2)	N(1)–Cu(1)–N(2)	81.5(2)
N(1)–Cu(1)–N(3)	81.0(2)	N(2)–Cu(1)–N(3)	83.8(2)
O(1)–Cu(2)–O(2)	80.7(1)	O(1)–Cu(2)–N(4)	111.8(1)
O(1)–Cu(2)–N(5)	96.3(2)	O(1)–Cu(2)–N(6)	165.2(2)
O(2)–Cu(2)–N(4)	108.9(1)	O(2)–Cu(2)–N(5)	170.4(2)
O(2)–Cu(2)–N(6)	96.9(2)	N(4)–Cu(2)–N(5)	80.7(2)
N(4)–Cu(2)–N(6)	82.8(2)	N(5)–Cu(2)–N(6)	83.7(2)
O(3)–Cu(3)–O(3)#1	81.3(2)	O(3)–Cu(3)–N(7)	104.7(2)
O(3)–Cu(3)–N(8)	172.9(2)	O(3)–Cu(3)–N(9)	98.3(2)
O(3)#1–Cu(3)–N(7)	111.2(2)	O(3)#1–Cu(3)–N(8)	94.9(2)
O(3)#1–Cu(3)–N(9)	167.5(2)	N(7)–Cu(3)–N(8)	82.3(2)
N(7)–Cu(3)–N(9)	81.1(2)	N(8)–Cu(3)–N(9)	84.2(2)
Cu(1)–O(1)–Cu(2)	94.7(1)	Cu(1)–O(2)–Cu(2)	97.0(1)
Cu(3)–O(3)–Cu(3)#1	98.7(2)		

[a] #1 = 1 − *x*, −*y*, −*z*.

angles for the planar $[Cu_2(\mu\text{-}OH)_2]^{2+}$ core are identical [98.7(2)°], however the Cu–O bonds are slightly different [1.933(4) *vs.* 1.969(4) Å]. Again, this may be due to H-bonding effects since both hydroxo groups form contacts to a water molecule [O(3) ··· O(16) = 2.87 Å] and a perchlorate anion [O(3) ··· O(10) = 3.06 Å].

The two L^{mes} ligands within the hexanuclear cation of **2** adopt "all-*cis*" conformations in which the three Cu(II)-tacn moieties attached to each mesitylene spacer reside on the same side of the plane defined by the aromatic ring. This contrasts with the "chair-like" conformation observed in **1** and leads to shorter Cu(1) ··· Cu(3) and Cu(2) ··· Cu(3) separations of 8.6 and 8.3 Å, respectively, when compared with **1**.

Complex **2** has some structural similarities to two hexanuclear Cu(II) complexes prepared by Karlin *et al.*[17] *via* oxygenation of the Cu(I) complex of a trinucleating derivative of bis(2-pyridylethyl)amine. These complexes also feature two triangular arrays, consisting of two flanking doubly-bridged sites and a central, "parallel-planar" di-μ-hydroxo-bridged site. A key difference, however, is that the flanking "dimers" in these complexes incorporate a phenoxo bridge between Cu(II) centres, formed by hydroxylation of mesitylene spacer on oxidation of the Cu(I) precursor compounds.

Magnetic properties

Magnetic susceptibility measurements were carried out on powdered samples of **1** and **2** in the temperature range 4.2–300 K. Samples were prepared from the crystal batches used in characterization studies and X-ray crystallography. Plots of magnetic moment (μ_{eff}) and magnetic susceptibility (χ_M) *versus* temperature are shown in Figs 3 and 4. For **1**, the μ_{eff} value decreases from 3.15 μ_B per Cu_3 unit (1.82 μ_B per Cu) at 300 K to 1.90 μ_B at 4.5 K (Fig. 3). This low temperature value identifies an $S = 1/2$ ground state, consistent with a system comprising an antiferromagnetically coupled copper(II) pair and a third magnetically independent copper(II) centre. The data were fitted using eqn. (1), in which the first (Bleaney–Bowers) term

$$x_M = (2N\beta^2g_1^2/kT)[3 + \exp(-2J_{12}/kT)]^{-1} + N\beta^2g_2^2/4kT + N\alpha \quad (1)$$

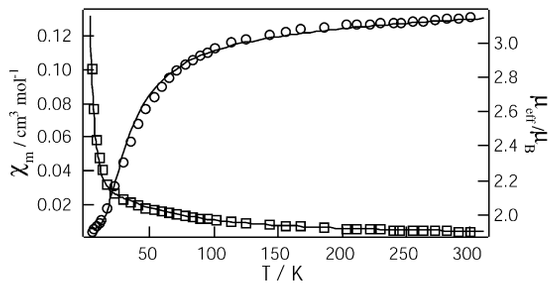

Fig. 3 Plot of χ_M (□) and μ_{eff} (○) (per Cu_3) *versus* temperature for complex **1**. The solid line shows the best-fit to eqn. (1) yielding g_1 = 2.013, g_2 = 2.216, $J_{12} = -24$ cm^{-1}, $N\alpha = 185 \times 10^{-6}$ cm^3 mol^{-1}.

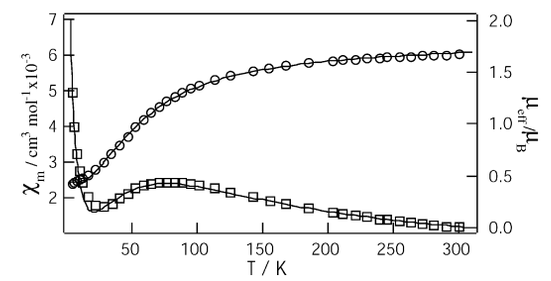

Fig. 4 Plot of χ_M (□) and μ_{eff} (○) (per Cu) *versus* temperature for complex **2**. The solid line shows the best-fit to eqn. (2) yielding g_1 = 2.070, g_2 = 1.970, $J_1 = -61$ cm^{-1}, $J_2 = -29$ cm^{-1}, $x = 0.06$, $N\alpha = 60 \times 10^{-6}$ cm^3 mol^{-1}.

accounts for the dihydroxo-bridged Cu(II) pair, and the second (Curie) term for the magnetically-isolated Cu(II) centre.

The parameters N, β and k in eqn. (1) have their usual meanings and $N\alpha$ is the temperature-independent paramagnetism. The g values of the dimer (g_1) and monomer (g_2) were assumed to be different. The least-squares fit of eqn. (1) to the data was of good quality, justifying the validity of the dimer-plus-monomer model, and yielded the parameters: g_1 = 2.013, g_2 = 2.216, $J_{12} = -24$ cm^{-1}, $N\alpha = 185 \times 10^{-6}$ cm^3 mol^{-1}. The negative value of the exchange coupling constant J_{12} is consistent with the presence of a weak antiferromagnetic interaction between the pair of hydroxo-bridged copper(II) centres.

The magnetic susceptibility of the "fully-bridged" system, **2**, shows a gradual increase with decreasing temperature, reaching a maximum at 76 K and then a minimum at 28 K (Fig. 4). Below this temperature, χ_M increases again due to the presence of a paramagnetic impurity of unknown origin. The maximum at 76 K is typical for antiferromagnetically-coupled systems. The corresponding plot of magnetic moment [per Cu(II)] *versus* temperature show a decrease from 1.69 μ_B at 300 K to 0.42 μ_B at 4.2 K. The presence of two different types of hydroxo-bridged copper(II) pairs in **2**, necessitated fitting of the data with eqn. (2). This models the system as three non-interacting dimers

$$\chi_M = [(1 - x)/6]\{(4N\beta^2g_1^2/kT)[3 + \exp(-2J_1/kT)]^{-1} + (2N\beta^2g_2^2/kT)[3 + \exp(-2J_2/kT)]^{-1}\} + xN\beta^2g_1^2/4kT + N\alpha \quad (2)$$

(two of which are the same) with different J values, J_1 and J_2, being assumed for the planar and "roof-shaped" cores, respectively.

A Curie–Weiss term was introduced to allow for a fraction (x) of paramagnetic impurity and χ_M is expressed per Cu(II). A good least-squares fit of eqn. (2) to the data was obtained using the parameters: g_1 = 2.070, g_2 = 1.970, $J_1 = -61$ cm^{-1}, $J_2 = -29$ cm^{-1}, $x = 0.06$, $N\alpha = 60 \times 10^{-6}$ cm^3 mol^{-1}. Interestingly, the value determined for the J_1 coupling constant indicates that the antiferromagnetic interaction between the Cu(II) centres of the "roof-shaped" $[Cu_2(\mu\text{-}OH)_2]^{2+}$ cores in **2** is stronger than in **1**.

Table 4 Structural and magnetic data for Cu(II) complexes with $Cu_2(\mu\text{-}OH)_2$ cores

Complex		Cu–O–Cu (φ/°)	Cu ··· Cu/Å	Cu–O/Å	δ^a/°	J/cm^{-1}
1	Bent core	98.9(2)	2.9041(8)	1.900(5)	152	−24
		92.1(1)		2.019(3)		
2	Bent core	94.7(1)	2.8757(8)	1.920(3)	153	−61
		97.0(1)		1.957(3)		
	Planar core	98.7(2)	2.961(1)	1.933(4)	180	−29
				1.969(4)		
$[Cu_2(Me_3tacn)_2(\mu\text{-}OH)_2](ClO_4)_2$ [b]		100.1(2)	2.971(1)	1.939(4)	180	−45
$[Cu_2(C_6H_{11}NH_2)_4(\mu\text{-}OH)_2](ClO_4)_2$ [c]		96.6(2)	2.934(8)	1.960(5)	148	−128
		99.7(2)		1.923(5)		
$[Cu_2(CH_3NH_2)_4(\mu OH)_2](SO_4)\cdot H_2O$ [d]		91.7(7)	2.782(5)	1.99(1)	133	−4
		88.6(7)		1.94(1)		
$[Cu_2L^{mx}(\mu\text{-}OH)_2](BPh_4)_2$ [e]		99.6(1)	2.9464(5)	1.931(2)	174	−80
$[Cu_4L^{dur}(\mu\text{-}OH)_4](ClO_4)_4$ [f]		97.9(4)	2.939(9)	1.961(8)	159	−27
		95.7(4)		1.975(8)		

[a] Dihedral angle between two CuO_2 planes. [b] Ref. 37, Me_3tacn = 1,4,7-trimethyl-1,4,7-triazacyclononane. [c] Ref. 5. [d] Ref. 6. [e] Ref. 38, L^{mx} = 1,3-bis(1,4,7-triazacyclonon-1-ylmethyl)benzene. [f] Ref. 33, L^{dur} = 1,2,4,5-tetrakis(1,4,7-triazacyclonon-1-ylmethyl)benzene.

Table 4 lists selected structural and magnetic data for complexes **1** and **2**, together with data for other related complexes. The J value calculated for the planar $[Cu_2(\mu\text{-}OH)_2]^{2+}$ core in **2** (−29 cm^{-1}) is close to the value of −43 cm^{-1} predicted from the J/φ correlation of Hodgson and Hatfield, $2J = -74.53\varphi + 7270$ cm^{-1}, where φ is the Cu–O–Cu angle[4,7] and in keeping with conclusions drawn from density functional calculations.[10] The coupling constant of −80 cm^{-1} reported for the near-planar complex, $[Cu_2L^{mx}(\mu\text{-}OH)_2](BPh_4)_2$, is more negative, as expected from the larger φ angle (J = –77 cm^{-1} calculated from J/φ correlation). In addition to φ, other angular distortions to the $LCu(\mu\text{-}OH)_2CuL$ unit may attenuate the value of J. Of relevance to this discussion is the finding of Charlot *et al.*[5,6] that the magnetic interaction becomes less antiferromagnetic at a given value of φ as the dihedral angle (δ) between the two Cu_2O planes is reduced from 180°. Thus, the weakest antiferromagnetic interaction is associated with the complex which has the smallest dihedral angle, *i.e.* $[Cu_2(CH_3NH_2)_4(\mu\text{-}OH)_2](SO_4)\cdot H_2O$.[6] The significantly more negative coupling constant for $[Cu_2(C_6H_{11}NH_2)_4(\mu\text{-}OH)_2](ClO_4)_2$,[5] than found for **1** and **2**, despite the similar δ angles in the compounds, is a reflection of the larger average Cu–O–Cu angle for the former (98.2°), since this would be expected to result in stronger antiferromagnetic coupling. A similar explanation can be provided for the slightly stronger coupling observed for the bent $[Cu_2(\mu\text{-}OH)_2]^{2+}$ cores in **2** (av. Cu–O–Cu = 95.9°) compared to that of **1** (av. Cu–O–Cu = 95.5°). Whilst it may appear surprising that the J value for $[Cu_2L^{mx}(\mu\text{-}OH)_2](BPh_4)_2$ [38] is more negative than that for the "roof-shaped" $[Cu_2(\mu\text{-}OH)_2]^{2+}$ cores in **1** and **2**, especially given the similarities in the supporting ligand structures, such a finding is, however, consistent with the significantly smaller δ angles observed in the latter two complexes.

Q-band EPR spectra

EPR spectra were measured at Q-band frequency on neat powdered and frozen glass (water–glycerol) samples of **1** (Fig. 5). The spectrum of the neat powder, at 290 K, showed very broad lines between 6000 and 13000 G, probably due to the coupled $Cu(OH)_2Cu$ unit superimposed on which were the four parallel Cu-hyperfine lines ($g_\parallel$ = 2.24 and $A_\parallel$ = 148 G) and a $g_\perp$ line at 2.03. Cooling to 6 K gave three well resolved lines at g = 2.26, 2.04 and 2.00, without hyperfine structure, indicative of rhombic symmetry being created at the uncoupled $Cu(tacn)(OH_2)_2$ moiety. Other trinuclear species have yielded rhombic signals.[39,40] No lines due to the $Cu(OH)_2Cu$ fragment were observed, in agreement with the magnetic data at this temperature. The frozen glass spectrum obtained at 120 K, showed an axial lineshape with $g_\parallel$ = 2.27 and $A_\parallel$ = 171 G and $g_\perp$ = 2.045, arising from the uncoupled $Cu(tacn)(OH_2)_2$ moiety. It should be noted that the solvent can influence the ligand-field symmetry around Cu in comparison to the powder spectrum, the latter being measured at much lower temperature. The ESR spectrum of **1** may be further complicated by the establishment of a pH dependent equilibrium with **2** and **3** in aqueous solution (or partly aqueous) (see Scheme 1). Nevertheless, the EPR data are generally compatible with the susceptibility data. A g value of 2.1 was obtained from the EPR results which compared to 2.21 from the susceptibility fits.

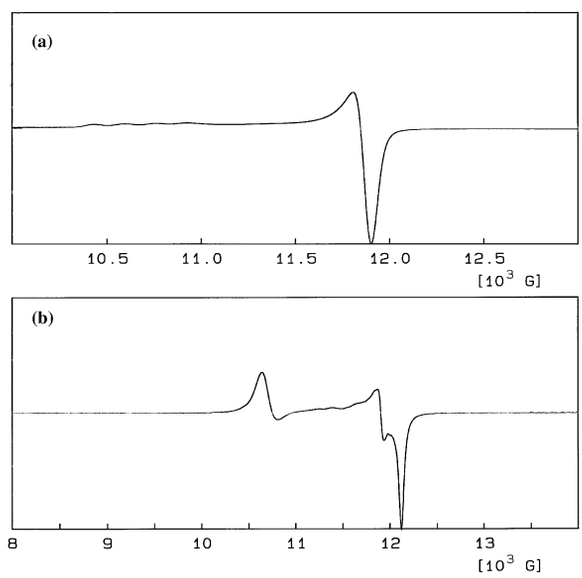

Fig. 5 Q-band EPR spectra (33.95 GHz) for complex **1** measured on: (a) a neat powdered sample, at 6 K; and (b) a frozen water–glycerol glass, at 120 K.

It is of interest to compare the present solid-state Q-band EPR spectra of **1** to those obtained for a related polymeric complex of L^{mes} containing trinuclear Cu units, subsequent to our publication.[25] This compound, $\{[Cu_3L(\mu\text{-}OH)(\mu_3\text{-}HPO_4)(H_2O)](PF_6)_3\cdot 3H_2O\}_n$, contains an HPO_4 bridge linking three Cu(II) centres from a $Cu(tacn)(OH_2)$ moiety and a $(tacn)Cu(OH)_2Cu(tacn)$ unit (Fig. 6). In that case, fitting of the magnetic data to an isosceles triangle model yielded an S = 1/2 ground state with J (μ-HPO_4^{2-}) = −90.3 cm^{-1} and J (μ-OH) = −53.4 cm^{-1}. The dimer plus monomer model gave a poorer fit.[25]

The Q-band spectra of a neat powder of $\{[Cu_3L(\mu\text{-}OH)(\mu_3\text{-}HPO_4)(H_2O)](PF_6)_3\cdot 3H_2O\}_n$ showed that as the temperature is lowered an asymmetric line at g = 2.076 becomes well resolved (see ESI †). At 4.7 K, an axial lineshape is clearly evident with a seven-line hyperfine pattern, the $g_\parallel$ resonance indicating one spin (S = 1/2) being delocalised between two Cu(II) ions (Fig. 7(a)). The lineshape was simulated very well using the Spin Hamiltonian parameters, g_z = 2.287, A_z = 85 G; g_x = 2.075,

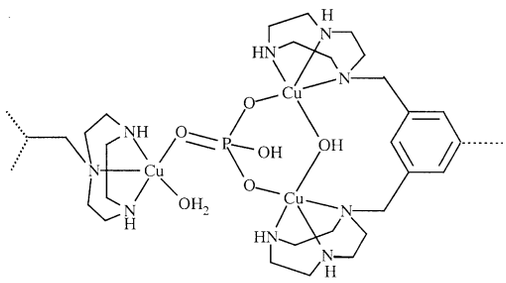

Fig. 6 Representation of the trinuclear Cu(II) units in $\{[Cu_3L(\mu\text{-}OH)(\mu_3\text{-}HPO_4)(H_2O)](PF_6)_3\cdot 3H_2O\}_n$.

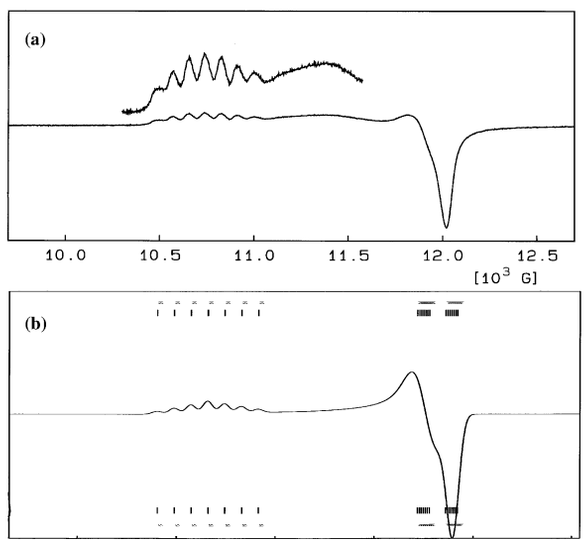

Fig. 7 (a) Q-band EPR spectrum (34.1 GHz) measured on a powder sample of $\{[Cu_3L(\mu\text{-}OH)(\mu_3\text{-}HPO_4)(H_2O)](PF_6)_3\cdot 3H_2O\}_n$ at 4.7 K; (b) Simulated Q-band spectrum (see also ref. 25 for X-band spectra measured on a powder and frozen DMF sample of this complex). The scale in (b) is the same as in (a) but slightly shifted.

A_x = 10 G; g_y = 2.050, A_y = 10 G; linewidths W_z = 50 G, W_x = 100 G, W_y = 50 G (Fig. 7(b). These parameters also simulated the published 9.6 GHz spectrum.[25] A broad line observed at 11500 G was not simulated and probably arises from trimer–trimer coupling. It increases in intensity as the temperature is increased. The precise origin of the 7-line copper hyperfine spectrum in the phosphate/hydroxo-bridged compound of L^{mes} is not clear,[25] since all three copper nuclei within the trinuclear repeat unit could potentially interact with the unpaired electron. The Cu(OH)Cu group is geometrically the most likely site for delocalization. In the present complex, **1**, the $Cu(OH)_2Cu$ group replaces the $Cu(OH)(HPO_4)Cu$ group in the phosphate complex, and, in contrast to the latter case, there is no bridging between trinuclear moieties. Thus, in the solid state the $Cu(tacn)(OH_2)_2$ fragment is isolated on the 'far side' of the mesityl ring and does not yield a seven-line pattern since the unpaired electron on this centre cannot interact with other Cu nuclear spins. Indeed, the nuclear hyperfine pattern of this fragment is not seen in the rhombic *g* components.

Acknowledgements

This work was supported by the Australian Research Council. B. G. was the recipient of an Australian Postgraduate Award.

References

1 D. J. Hodgson, *Prog. Inorg. Chem.*, 1975, **19**, 173.
2 C. J. Cairns and D. H. Busch, *Coord. Chem. Rev.*, 1986, **1**, 55.
3 W. E. Hatfield, in *Magneto-Structural Correlations in Exchange Coupled Systems,* ed. R. D. Willett, D. Gatteschi and O. Kahn, NATO-ASI Series D, Reidel, Dordrecht, 1984, p. 555.
4 V. H. Crawford, H. W. Richardson, J. R. Wasson, D. J. Hodgson and W. E. Hatfield, *Inorg. Chem.*, 1976, **15**, 2107.
5 M. F. Charlot, S. Jeannin, Y. Jeannin, O. Kahn, J. Lucrece-Aubal and J. S. Martin-Frere, *Inorg. Chem.*, 1979, **18**, 1675.
6 M. F. Charlot, O. Kahn, S. Jeannin and Y. Jeannin, *Inorg. Chem.*, 1980, **19**, 1410.
7 D. J. Hodgson, *J. Mol. Catal.*, 1984, **23**, 219.
8 M. S. Haddad, S. P. Wilson, D. J. Hodgson and D. N. Hendrickson, *J. Am. Chem. Soc.*, 1981, **103**, 384.
9 A. Escuer, R. Vicente and J. Ribas, *Polyhedron*, 1992, **11**, 453.
10 E. Ruiz, P. Alemany, S. Alvarez and J. Cano, *J. Am. Chem. Soc.*, 1997, **119**, 1297 and references therein.
11 K. D. Karlin, Z. Tyeklár and A. D. Zuberbühler, in *Bio-inorganic Catalysis*, ed. J. Reedjik, Marcel Dekker Inc., New York, 1993, p. 261.
12 V. McKee, *Adv. Inorg. Chem.*, 1993, **40**, 323.
13 N. Kitajima and Y. Moro-oka, *Chem. Rev.*, 1994, **94**, 737.
14 J. P. Klinman, *Chem. Rev.*, 1996, **96**, 2541; E. I. Solomon, U. M. Sundaram and T. E. Machonkin, *Chem. Rev.*, 1996, **96**, 2563; B. Wallar and J. D. Lipscomb, *Chem. Rev.*, 1996, **96**, 2625 and references therein.
15 K. D. Karlin, S. Kaderli and A. Zuberbühler, *Acc. Chem. Res.*, 1997, **30**, 139.
16 W. B. Tolman, *Acc. Chem. Res.*, 1997, **30**, 139; S. Mehapatra, S. Kaderli, A. Llobet, Y.-M. Neuhold, T. Palanch, J. A. Halfen, V. G. Young, Jr., T. A. Kaden, L. Que, Jr., A. D. Zuberbühler and W. R. Tolman, *Inorg. Chem.*, 1997, **36**, 6343 and references therein.
17 K. D. Karlin, Q.-F. Gan, A. Farooq, S. Liu and J. Zubieta, *Inorg. Chem.*, 1990, **29**, 2549.
18 P. Chaudhuri, I. Karpenstein, M. Winter, C. Butzlaff, E. Bill, A. X. Trautwein, U. Flörke and H.-J. Haupt, *Chem. Commun.*, 1992, 321.
19 D. E. Fenton, in *Perspectives in Coordination Chemistry*, ed. A. F. Williams, C. Floriani and A. E. Merbach, Verlag Helvetica Chemica Acta, Basel, Germany, 1992, p. 203.
20 D. E. Fenton and H. Okawa, *J. Chem. Soc., Dalton Trans.*, 1993, 1349.
21 H. Adams, N. A. Bailey, M. J. S. Dwyer, D. E. Fenton, P. C. Hellier, P. D. Hempstead and J. M. Latour, *J. Chem. Soc., Dalton Trans.*, 1993, 1207.
22 S. Meenakumari, S. K. Tiwary and A. R. Chakravarty, *Inorg. Chem.*, 1994, **33**, 2085.
23 P. Hubberstey and C. E. Russell, *J, Chem. Soc., Chem. Commun.*, 1995, 959.
24 A. P. Cole, D. E. Root, P. Mukherjee, E. I. Solomon and T. D. P. Stack, *Science*, 1996, **273**, 1848.
25 L. Spiccia, B. Graham, M. T. W. Hearn, G. Lazarev, B. Moubaraki, K. S. Murray and E. R. T. Tiekink, *J. Chem. Soc., Dalton Trans*, 1997, 4089.
26 S. Yamanaka, H. Okawa, K.-I. Motoda, M. Yonemura, D. E. Fenton, M. Ebadi and A. P. B. Lever, *Inorg. Chem.*, 1999, **38**, 1825.
27 R. Parker, D. C. R. Hockless, B. Moubaraki, K. S. Murray and L. Spiccia, *Chem. Commun.*, 1996, 2789.
28 B. Graham, L. Spiccia, B. Moubaraki, K. S. Murray, J. D. Cashion and D. C. R. Hockless, *J. Chem. Soc., Dalton Trans.*, 1997, 887.
29 S. J. Brudenell, A. M. Bond, L. Spiccia, P. Comba and D. C. R. Hockless, *Inorg. Chem.*, 1998, **37**, 3705.
30 S. J. Brudenell, L. Spiccia, D. C. R. Hockless and E. R. T. Tiekink, *J. Chem. Soc., Dalton Trans.*, 1999, 1475–1482.
31 S. J. Brudenell, L. Spiccia, A. M. Bond, G. D. Fallon, P. J. Mahon, D. C. R. Hockless and E. R. T. Tiekink, *Inorg. Chem.*, 2000, **39**, 881.
32 B. Graham, M. J. Grannas, M. T. W. Hearn, C. M. Kepert, L. Spiccia, B. W. Skelton and A. H. White, *Inorg. Chem.*, 2000, **39**, 1092.
33 B. Graham, M. T. W. Hearn, P. C. Junk, C. M. Kepert, F. E. Mabbs, B. Moubaraki, K. S. Murray and L. Spiccia, *Inorg. Chem.*, 2001, **40**, 1536.
34 teXsan: Crystal Structure Analysis Package, Molecular Structure Corporation, Houston, TX, 1992.
35 B. J. Hathaway, in *Comprehensive Coordination Chemistry*, ed. G. Wilkinson, R. D. Gillard and J. A. McCleverty, Pergamon Press, Oxford, England, 1987, p. 533.
36 A. W. Addison, T. N. Rao, J. Reedijk, J. van Rijn and G. C. Verschoor, *J. Chem. Soc., Dalton Trans.*, 1984, 1349.
37 P. Chaudhuri, D. Ventur, K. Wieghardt, E.-M. Peters, K. Peters and A. Simon, *Angew. Chem., Int. Ed. Engl.*, 1985, **24**, 57.
38 L. J. Farrugia, P. A. Lovatt and R. P. Peacock, *J. Chem. Soc., Dalton Trans.*, 1997, 911.
39 P. Chaudhuri, M. Winter, B. P. C. Della Vedova, E. Bill, A. Trautwein, S. Gehring, P. Fleisschhauer, B. Nuber and J. Weiss, *Inorg. Chem.*, 1991, **30**, 2148.
40 R. Veit, J.-J. Girerd, O. Kahn, F. Robert and Y. Jeannin, *Inorg. Chem.*, 1986, **25**, 4175.